

## Atlantic Ocean CO<sub>2</sub> uptake reduced by weakening of the meridional overturning circulation

Fiz F. Pérez<sup>1,\*</sup>, Herlé Mercier<sup>2</sup>, Marcos Vázquez-Rodríguez<sup>1</sup>, Pascale Lherminier<sup>3</sup>, Anton Velo<sup>1</sup>, Paula C. Pardo<sup>1</sup>, Gabriel Rosón<sup>4</sup> and Aida F. Ríos<sup>1</sup>

<sup>1</sup> Instituto de Investigaciones Marinas, IIM-CSIC, 36208 Vigo, Spain

<sup>2</sup> CNRS, Laboratoire de Physique des Océans, UMR6523, CNRS, Ifremer, IRD, UBO, 29280 Plouzané, France

<sup>3</sup> Ifremer, Laboratoire de Physique des Océans, UMR6523, CNRS, Ifremer, IRD, UBO, 29280 Plouzané, France

<sup>4</sup> Faculty of Marine Sciences, University of Vigo, Campus Lagoas-Marcosende, 36200 Vigo, Spain

\*: Corresponding author : Fiz F. Pérez, email address : [fiz.perez@iim.csic.es](mailto:fiz.perez@iim.csic.es)

### Abstract:

Uptake of atmospheric carbon dioxide in the subpolar North Atlantic Ocean declined rapidly between 1990 and 2006. This reduction in carbon dioxide uptake was related to warming at the sea surface, which—according to model simulations—coincided with a reduction in the Atlantic meridional overturning circulation. The extent to which the slowdown of this circulation system—which transports warm surface waters to the northern high latitudes, and cool deep waters south—contributed to the reduction in carbon uptake has remained uncertain. Here, we use data on the oceanic transport of volume, heat and carbon dioxide to track carbon dioxide uptake in the subtropical and subpolar regions of the North Atlantic Ocean over the past two decades. We separate anthropogenic carbon from natural carbon by assuming that the latter corresponds to a pre-industrial atmosphere, whereas the remaining is anthropogenic. We find that the uptake of anthropogenic carbon dioxide—released by human activities—occurred almost exclusively in the subtropical gyre. In contrast, natural carbon dioxide uptake—which results from natural Earth system processes—dominated in the subpolar gyre. We attribute the weakening of contemporary carbon dioxide uptake in the subpolar North Atlantic to a reduction in the natural component. We show that the slowdown of the meridional overturning circulation was largely responsible for the reduction in carbon uptake, through a reduction of oceanic heat loss to the atmosphere, and for the concomitant decline in anthropogenic CO<sub>2</sub> storage in subpolar waters.

### 1. Introduction

Contemporary CO<sub>2</sub> uptake from the atmosphere by the global ocean has been estimated to be  $1.6 \pm 0.9 \text{ PgC yr}^{-1}$  from an observation-based CO<sub>2</sub> flux climatology<sup>1</sup> referenced to the year 2000. Contemporary atmospheric CO<sub>2</sub> consists of a mix of molecularly identical natural and anthropogenic CO<sub>2</sub> (C<sub>ANT</sub>). The whole North Atlantic (from the Equator to the Bering Strait, including the Arctic seas) represents only 13% of the global ocean area and yet annually accounts for about one-third of the contemporary ocean CO<sub>2</sub> uptake ( $0.47 \text{ PgC yr}^{-1}$ ) and has the largest of C<sub>ANT</sub> storage rates ( $0.49 \pm 0.04 \text{ PgC yr}^{-1}$  referenced to 2004) of all oceans<sup>2</sup>. However, air–sea CO<sub>2</sub> uptake in the North Atlantic is not necessarily predominantly anthropogenic<sup>3, 4</sup>. In fact, air–sea CO<sub>2</sub> fluxes in the North Atlantic result from anthropogenic forcing and progressive northward cooling of the upper limb of the meridional overturning circulation

40 (MOC). The latter is responsible for the NA uptake of natural CO<sub>2</sub> (ref. 5) that would occur even in the  
41 absence of the anthropogenic forcing. This air-sea flux of natural CO<sub>2</sub> is driven by thermal processes<sup>5</sup>  
42 — not biological processes — and has been estimated in 0.31-0.39 PgC·y<sup>-1</sup> (refs 5,6), which represents  
43 roughly three-fourths of the contemporary air-sea CO<sub>2</sub> uptake. The remaining uptake (0.08-0.16 PgC·y<sup>-1</sup>)  
44 comes from the anthropogenic perturbation, which alone cannot account for the C<sub>ANT</sub> storage rate of  
45 the NA<sup>2</sup>. The additional source of C<sub>ANT</sub> comes from the northward transport of C<sub>ANT</sub>-laden south-  
46 latitude waters<sup>4,7-9</sup> by the upper limb of the MOC.

47 Air-sea CO<sub>2</sub> fluxes in the subpolar and subtropical regions have similar rates (0.27 and 0.22  
48 PgC·y<sup>-1</sup>, referenced to 2000, respectively<sup>1</sup>), but the flux per unit area in the subpolar NA is twice that in  
49 the subtropical NA (2.0 vs. 1.0 mol·C·m<sup>-2</sup>·y<sup>-1</sup>). At multidecadal time scales, sea surface pCO<sub>2</sub> in these  
50 regions follow the atmospheric increase<sup>1</sup>. However, these two regions also have contrasting responses  
51 to different North Atlantic Oscillation (NAO) periods. Between 1993 and 2006, the CO<sub>2</sub> uptake rate in  
52 the western subpolar<sup>10</sup> and, more generally, in the subpolar gyre<sup>11</sup> dramatically weakened as evidenced  
53 by the rapid increase in sea-surface pCO<sub>2</sub> compared to atmospheric pCO<sub>2</sub>. Changes in the NAO (the  
54 index declined from high positive values in the early 1990s to lower values in the early 2000s)<sup>12</sup> and  
55 the associated weakening of the northward transport of subtropical water by the North Atlantic Current  
56 (NAC) have been identified, using inverse atmospheric CO<sub>2</sub> and physical-biological models<sup>13,14</sup>, as the  
57 main causes for the decrease in CO<sub>2</sub> uptake in the subpolar NA. In contrast, in the subtropical NA, CO<sub>2</sub>  
58 uptake increased during the years with low NAO index<sup>15,16</sup>. There are, however, few observations of  
59 C<sub>ANT</sub> transport reported for different NAO conditions. In addition, numerical models have shown  
60 contrasting CO<sub>2</sub> uptake responses<sup>14,17</sup> and discrepancies with field data, suggesting that more  
61 observations are required to better understand the interactions between ocean circulation and the carbon

62 cycle, in particular regarding the mechanisms governing the exchange, advection and accumulation of  
63 CO<sub>2</sub>.

64

### 65 **CO<sub>2</sub> transport by the meridional overturning circulation**

66 The analysis of repeated trans-Atlantic sections at 25°N showed that the upper limb of the MOC  
67 carries  $18.7 \pm 2.1$  Sv ( $\text{Sv} = 10^6 \text{ m}^3 \cdot \text{s}^{-1}$ ) northwards<sup>18</sup> (northward transport is considered positive). Most  
68 of this transport occurs through the Gulf Stream and, downstream, through the NAC (Fig. 1). The warm  
69 water moving northward in the upper limb of the MOC has high concentrations of C<sub>ANT</sub> ([C<sub>ANT</sub>]),  
70 whereas the cold, deep water moving southward<sup>4,7</sup> has very low [C<sub>ANT</sub>]. This pattern yields net  
71 northward transports of heat<sup>19</sup> and C<sub>ANT</sub> of 1-1.3 PW and 0.19-0.23 PgC·y<sup>-1</sup> (refs 4, 7), respectively. The  
72 overturning and the southward transport of deep water of the MOC happen in the northern NA and  
73 Nordic seas, where high wintertime heat loss generates vertical convection and produces cold, fresh  
74 and well-ventilated deep waters<sup>20</sup> that are entrained in the deep western boundary current. Recent  
75 estimations of the MOC across the repeated A25 section (Greenland to Portugal; Fig. 1) showed  
76 slightly weaker mass transports<sup>21,22</sup> (12-18.5 Sv) than at 25°N. The upper and lower limbs of the MOC  
77 showed contrasting temperatures and [C<sub>ANT</sub>] (Fig 1b, see Methods for details on C<sub>ANT</sub> computations),  
78 but both properties are positively correlated. The small westward increase in [C<sub>ANT</sub>] at constant  
79 temperature indicates recent ventilation of the western side of the section. In the surface layer, [C<sub>ANT</sub>] is  
80 close to saturation. East of the NAC, the low values ( $< 10 \mu\text{mol} \cdot \text{kg}^{-1}$ ) in deep waters create a larger  
81 vertical gradient of C<sub>ANT</sub> between the surface and the deep ocean than to the west of the NAC, *i.e.* in  
82 the subpolar region, where the Labrador Sea Water (LSW), the Denmark Strait Overflow Water and the  
83 Iceland-Scotland Overflow Water show moderate [C<sub>ANT</sub>].

84 Numerical models have shown that NAO conditions influence air-sea CO<sub>2</sub> uptake in the NA<sup>13</sup>  
85 by modulating the strength with which the NAC carries subtropical waters into the subpolar gyre<sup>14</sup>.  
86 However, these results have not been confronted with measurements of volume, heat and CO<sub>2</sub>  
87 transports due to the lack of observations during different NAO conditions. We examined several  
88 occupations of the A25 Greenland-Portugal section (Fig. 1a) conducted in August 1997 (FOUREX  
89 cruise) and in June 2002, 2004 and 2006 (OVIDE cruises). The year 1997 came after an unusually long  
90 high NAO period followed by a period of lower NAO between 2002 and 2006. The A25 cruise was  
91 specifically designed to run perpendicularly across the main NA currents (the different branches of the  
92 NAC and the boundary currents linked to the topography) in order to minimize the transports due to  
93 eddies<sup>23</sup>. Measurements from these cruises were used to calculate MOC<sub>σ</sub> transport<sup>21,22,24</sup>, taking σ<sub>1</sub>  
94 (density anomaly referenced to 1000 dbar) as the vertical coordinate (Fig. 2). MOC<sub>σ</sub>, varied from  
95 20.5±2.2 Sv in 1997 to the average value of 14.6±1.7 Sv for the 2002-2006 period (see Methods and  
96 Supplementary Information for details on the removal of the seasonal cycle and the computation of the  
97 uncertainties). When integrated from Greenland to Portugal along constant σ<sub>1</sub>-lines, heat and C<sub>ANT</sub>  
98 transports resemble the vertical profiles of the overturning circulation (Fig. 2). Volume, heat and C<sub>ANT</sub>  
99 transport profiles are highly correlated (0.92>r<sup>2</sup>>0.89), because the upper limb of the MOC transports  
100 warmer waters with higher [C<sub>ANT</sub>] than the lower limb. On average, the net volume transport is  
101 negligible, and there is a net northward transport of heat (0.59±0.09 PW) and C<sub>ANT</sub> (0.092±0.010  
102 PgC·y<sup>-1</sup>). In 1997, the circulation showed a strong southward volume transport at intermediate levels  
103 (32.4<σ<sub>1</sub><32.5) that corresponds to the layer of the classical LSW (Fig. 2). On the other hand, during  
104 the lower NAO period, the southward volume transport was slightly stronger in the layer of the upper  
105 LSW (32.2<σ<sub>1</sub><32.3)<sup>20</sup>. In addition, the upper limb of MOC<sub>σ</sub> (σ<sub>1</sub><32.1) showed a stronger transport in  
106 1997 than in 2002-2006 (Fig. 2a), which is attributed to the NAC variability<sup>24</sup>. The heat and C<sub>ANT</sub>

107 transports in 2002-2006 ( $0.41\pm 0.06$  PW and  $0.074\pm 0.009$  PgC $\cdot$ y $^{-1}$ ) were lower than in 1997 ( $0.76\pm 0.09$   
108 PW and  $0.110\pm 0.012$  PgC $\cdot$ y $^{-1}$ ). Most remarkably, although the weakening of MOC $_{\sigma}$  and of C $_{ANT}$   
109 transport were very similar (29% and 33%, respectively), heat transport underwent a more dramatic  
110 reduction (46%) between 1997 and 2002-2006. This contrasting behavior of volume and heat transports  
111 agrees with results from high-resolution circulation models<sup>25</sup>. We will treat the observations obtained in  
112 1997 as a case study of circulation linked to a high NAO period, as opposed to the measurements  
113 obtained during 2002-2006 that were associated with a low/neutral NAO period.

114

### 115 **Anthropogenic CO<sub>2</sub> budget of the North Atlantic**

116 The C $_{ANT}$  budget of any oceanic region is the result of the balance between lateral advection,  
117 air-sea fluxes and storage rates. Hereinafter, we will refer to the NA as the region extending from 25°N  
118 to the Bering Strait. We calculated the NA C $_{ANT}$  budget referenced to 2004 from updated datasets and  
119 for four different subregions or boxes (Fig. 3). In the subtropical box, the C $_{ANT}$  storage rate was  
120 computed as described in the Methods section, while the estimates in other boxes were obtained from  
121 the literature (Supplementary Information). For the NA, we obtained a storage rate of  $0.386\pm 0.012$   
122 PgC $\cdot$ y $^{-1}$  ( $0.95\pm 0.05$  mol-C $\cdot$ m $^{-2}\cdot$ y $^{-1}$ ) consistent with previous results ( $0.39\pm 0.02$  PgC $\cdot$ y $^{-1}$ , referenced to  
123 2004; ref. 26). The C $_{ANT}$  transports at 25°N (refs 4,7) were updated from 1992 and 1998 to 2004,  
124 resulting on a mean value of  $0.25\pm 0.05$  PgC $\cdot$ y $^{-1}$  (Methods section) that is consistent with a long term  
125 average MOC (ref. 18). Comparatively, C $_{ANT}$  transport in the Bering Strait is low ( $0.008\pm 0.003$  PgC $\cdot$ y $^{-1}$   
126 <sup>1</sup>)<sup>7,26</sup>. Closing the C $_{ANT}$  budget in the NA, an air-sea C $_{ANT}$  flux of  $0.13\pm 0.05$  PgC $\cdot$ y $^{-1}$  was inferred. This  
127 estimate is compatible with the value of  $0.17\pm 0.06$  PgC $\cdot$ y $^{-1}$  (rescaled to 2004) derived from  $\delta^{13}\text{C}$   
128 observations<sup>9</sup>. Overall, these results indicate that the net advective transports contribute to  $65\pm 13\%$  of  
129 the NA C $_{ANT}$  storage rate (Fig. 3). Importantly, our observation-based estimate of the contribution of

130 lateral transports to the  $C_{\text{ANT}}$  storage rate is larger than the 30% obtained by ocean inversions that  
131 combine  $C_{\text{ANT}}$  observations with transports and mixing from GCMs (ref. 26). By way of contrast, our  
132 result is consistent with a biogeochemical model<sup>27</sup> that predicted larger northward  $C_{\text{ANT}}$  transports than  
133 ocean inversions in the NA. Subtracting our estimate of air-sea  $C_{\text{ANT}}$  flux from the contemporary  $\text{CO}_2$   
134 uptake for the NA ( $0.49 \text{ PgC}\cdot\text{y}^{-1}$ ; ref. 1), we obtained a natural  $\text{CO}_2$  uptake of  $0.36 \text{ PgC}\cdot\text{y}^{-1}$ , thereby  
135 corroborating independent estimates<sup>5,6</sup>. The air-sea  $C_{\text{ANT}}$  flux represents about 26% of the  
136 contemporary air-sea  $\text{CO}_2$  uptake, which is much smaller than the 63% obtained from oceanic  
137 inversions<sup>3</sup>. The relevance of our result is that the air-sea  $C_{\text{ANT}}$  and natural  $\text{CO}_2$  uptake estimates from  
138 the  $C_{\text{ANT}}$  budget are consistent with independent  $^{13}\text{C}/^{12}\text{C}$  observations<sup>9</sup> and with other estimates of the  
139 air-sea natural  $\text{CO}_2$  uptake<sup>5,6</sup>.

140 The  $C_{\text{ANT}}$  storage rate estimated for the subtropical box is  $0.280\pm 0.011 \text{ PgC}\cdot\text{y}^{-1}$  ( $1.41\pm 0.05 \text{ mol}\cdot$   
141  $\text{C}\cdot\text{m}^{-2}\cdot\text{y}^{-1}$ ). So the subtropical box contributes 73% of the NA  $C_{\text{ANT}}$  storage rate, even though it  
142 represents only 49% of the NA area. By closing the  $C_{\text{ANT}}$  budget for this box (Fig. 3), we inferred an  
143 air-sea  $C_{\text{ANT}}$  uptake of  $0.12\pm 0.05 \text{ PgC}\cdot\text{y}^{-1}$  ( $0.60\pm 0.25 \text{ mol}\cdot\text{C}\cdot\text{m}^{-2}\cdot\text{y}^{-1}$ ). Here, the air-sea  $C_{\text{ANT}}$  flux is  
144 predominant in the contemporary air-sea  $\text{CO}_2$  flux ( $1.0 \text{ mol}\cdot\text{C}\cdot\text{m}^{-2}\cdot\text{y}^{-1}$ ). It represents 92% of the NA air-  
145 sea  $C_{\text{ANT}}$  uptake. In contrast, in the subpolar box, the  $C_{\text{ANT}}$  storage rate per unit area ( $0.99\pm 0.06 \text{ mol}\cdot$   
146  $\text{C}\cdot\text{m}^{-2}\cdot\text{y}^{-1}$ ) amounts to ~70% of that in the subtropical box<sup>28</sup>. To derive the  $C_{\text{ANT}}$  budget for the subpolar  
147 box, the  $C_{\text{ANT}}$  lateral transport over the Nordic sills ( $0.063\pm 0.019 \text{ PgC}\cdot\text{y}^{-1}$ ) was calculated from  
148 available volume transports<sup>22,29</sup> and from  $[C_{\text{ANT}}]$  estimated from water mass ages and mixing models<sup>30</sup>  
149 (Supplementary Information). Then, the air-sea  $C_{\text{ANT}}$  flux was estimated at  $0.016\pm 0.012 \text{ PgC}\cdot\text{y}^{-1}$ ,  
150 which represents 35% of the  $C_{\text{ANT}}$  storage rate in this box. The air-sea  $C_{\text{ANT}}$  flux per unit area in the  
151 subpolar box ( $0.36\pm 0.25 \text{ mol}\cdot\text{C}\cdot\text{m}^{-2}\cdot\text{y}^{-1}$ ) is about 60% of the subtropical box which gives to the  
152 subtropical box a prevailing role in  $C_{\text{ANT}}$  uptake. Furthermore, the contemporary air-sea  $\text{CO}_2$  uptake

153 per unit area ( $2.0 \text{ mol-C} \cdot \text{m}^{-2} \cdot \text{y}^{-1}$ ) in the subpolar box is 5 times higher than the air-sea  $C_{\text{ANT}}$  uptake. This  
154 means that the natural component largely prevails over the anthropogenic component in the subpolar  
155 box. Interestingly, this result is in contrast with the subtropical box, where the air-sea anthropogenic  
156 flux is the major component (~60%).

157 The net heat and  $C_{\text{ANT}}$  transports flowing into the Nordic Seas reach  $0.25 \pm 0.05 \text{ PW}$  and  
158  $0.063 \pm 0.019 \text{ PgC} \cdot \text{y}^{-1}$ , respectively (Fig. 3, Supplementary Information). The  $C_{\text{ANT}}$  lateral transport  
159 almost fully accounts for the  $C_{\text{ANT}}$  storage rate in the Nordic<sup>31</sup> and Arctic Seas<sup>32</sup> meaning that air-sea  
160  $C_{\text{ANT}}$  fluxes are practically zero (Fig. 3). Analyses based on  $^{13}\text{C}/^{12}\text{C}$  measurements<sup>33,34</sup> have determined  
161 that the upper waters entering the Nordic Seas are saturated with  $C_{\text{ANT}}$ , preventing any further  $C_{\text{ANT}}$   
162 uptake from the atmosphere and possibly causing outgassing due to the decline in buffering capacity.  
163 The strong air-sea heat loss in the Nordic and Arctic Seas actually drives the uptake of natural  $\text{CO}_2$ , as  
164 corroborated by observations in climatological analyses<sup>1</sup> that indicate a high air-sea  $\text{CO}_2$  uptake ( $2.0$   
165  $\text{ mol-C} \cdot \text{m}^{-2} \cdot \text{y}^{-1}$ ) north of  $50^\circ\text{N}$ . In summary, while heat loss causes a strong natural  $\text{CO}_2$  uptake in the  
166 Nordic and Arctic regions, the low anthropogenic component is less affected by the air-sea heat fluxes.

167

### 168 **North Atlantic oscillation impact on $\text{CO}_2$ fluxes**

169 The subpolar gyre is a remarkably rapid entrance portal for  $C_{\text{ANT}}$  into the deep ocean due to  
170 deep convection. In the early 1990s, the highly positive NAO period coincided with exceptional  
171 convection activity in the Labrador<sup>20,35</sup> and Irminger<sup>36</sup> Seas. Between 1997 and 2003, lower LSW  
172 formation rates prompted a decrease of  $20 \text{ mol-C} \cdot \text{m}^{-2}$  in the  $C_{\text{ANT}}$  inventory, as inferred from  
173 chlorofluorocarbon data<sup>37</sup>. In the subpolar box, the  $C_{\text{ANT}}$  storage rate dropped from  $0.083 \pm 0.008$  during  
174 high NAO conditions in 1997 to  $0.026 \pm 0.004 \text{ PgC} \cdot \text{y}^{-1}$  during the 2002-2006 low NAO period<sup>28</sup>. Hence,  
175  $C_{\text{ANT}}$  storage rates per unit area were nearly three times lower during low NAO than high NAO periods

176 (Fig. 4). The decrease in northward  $C_{ANT}$  transport (Fig. 4) that followed the high-to-low NAO  
177 transition (from  $0.110$  to  $0.074 \text{ PgC}\cdot\text{y}^{-1}$ ) is strongly related to the weakening of the intensity of the  
178 MOC (from  $20.5\pm 2.2$  to  $14.6\pm 1.7 \text{ Sv}$ ). Most remarkably, the converging  $C_{ANT}$  lateral transports in the  
179 subpolar box decreased from  $0.053\pm 0.021$  to  $0.011\pm 0.020 \text{ PgC}\cdot\text{y}^{-1}$ . In these estimations, we assumed  
180 that the volume transport over the Nordic sills was constant, as suggested by observations<sup>29</sup>, and  $[C_{ANT}]$   
181 was time-rescaled using a rate of increase of  $1.6\% \text{ y}^{-1}$  (Supplementary Information). After these  
182 calculations, the inferred air-sea  $C_{ANT}$  flux for the subpolar region was  $0.53\pm 0.22 \text{ mol}\cdot\text{C}\cdot\text{m}^{-2}\cdot\text{y}^{-1}$  during  
183 the high NAO period and  $0.33\pm 0.25 \text{ mol}\cdot\text{C}\cdot\text{m}^{-2}\cdot\text{y}^{-1}$  during the low NAO period. During the low NAO  
184 period, the  $C_{ANT}$  storage rate decreased due to the decrease in  $C_{ANT}$  lateral transport associated with the  
185 weakening of the MOC. Our results also suggest that this decrease was associated with a weakening in  
186 the air-sea  $C_{ANT}$  uptake.

187         The variability of the air-sea  $\text{CO}_2$  flux in the subpolar gyre has already been described, modeled  
188 and discussed in regard to NAO variability<sup>13,14,38,39</sup>. In the north-western subpolar gyre, a reduction in  
189 the contemporary air-sea  $\text{CO}_2$  flux of  $\sim 1.2 \text{ mol}\cdot\text{C}\cdot\text{m}^{-2}\cdot\text{y}^{-1}$  was observed between 1993-94 and 2003-05  
190 (refs 11, 38) and numerical simulation linked it to the weakening of the advection of subtropical waters  
191 with low total inorganic  $\text{CO}_2$  ( $C_T$ ) into the subpolar gyre<sup>14</sup>. This weakening is in agreement with our  
192 results (Fig. 4). During high NAO periods, heat loss increased<sup>40</sup>, favouring the decrease in the surface  
193  $\text{pCO}_2$ . The opposite is true during low NAO periods. Assuming a constant heat flux of  $0.25\pm 0.05 \text{ PW}$   
194 over the sills<sup>29</sup>, we inferred, from the heat budget, a heat loss that is 1.5 to 3 times higher during high  
195 NAO than during low NAO periods (Fig. 4). Using the relationship between heat loss and natural  $\text{CO}_2$   
196 flux (see Methods), we inferred a decrease in the air-sea flux of natural  $\text{CO}_2$  of  $3.0\pm 1.0$  to  $1.7\pm 1.0 \text{ mol}\cdot\text{C}\cdot\text{m}^{-2}\cdot\text{y}^{-1}$   
197 ( $0.13$  to  $0.05 \text{ PgC}\cdot\text{y}^{-1}$ , Fig. 4). This estimate is compatible with the rate of decrease in air-sea  
198  $\text{CO}_2$  fluxes in the subpolar gyre ( $2.3$  to  $1.0 \text{ mol}\cdot\text{C}\cdot\text{m}^{-2}\cdot\text{y}^{-1}$ ) reported from surface observations<sup>39</sup>. Most

199 importantly, this result strongly suggests that variability in the air-sea flux of natural CO<sub>2</sub> over the  
200 subpolar gyre responds to variability in the advection of subtropical waters with low [C<sub>T</sub>] and can be  
201 determined from the air-sea heat flux.

202         A possible explanation for the contrasting behaviour of the subtropical and subpolar regions lies  
203 in the origin of the water masses crossing the Florida Strait where ~45% of the volume transport comes  
204 from the South Atlantic as warm and intermediate waters<sup>41</sup> with low [C<sub>ANT</sub>] (ref. 4). These low [C<sub>ANT</sub>]  
205 waters are part of the upper limb of the MOC and reach C<sub>ANT</sub> saturation levels on their path to the  
206 subpolar gyre. They incorporate about 0.08 PgC·y<sup>-1</sup>, which represents two thirds of the air-sea C<sub>ANT</sub>  
207 flux in the subtropical box and contributes to the local response to anthropogenic forcing (Fig. 3). This  
208 explains why the air-sea C<sub>ANT</sub> flux in the subtropical region is higher than that observed in the subpolar  
209 region. Furthermore, the intermediate water flowing through the Florida Strait is oversaturated with  
210 natural CO<sub>2</sub> (~30 μmol·kg<sup>-1</sup>) due to biological remineralization<sup>4</sup>. This allows the waters in the upper  
211 limb of the MOC to remain CO<sub>2</sub>-saturated with low additional atmospheric uptake, despite the ~7°C  
212 cooling undergone as they travel through the subtropical box, thereby explaining the low natural air-sea  
213 CO<sub>2</sub> flux in this box.

214         In summary, our results give a coherent and observation-based understanding of the CO<sub>2</sub> budget  
215 in NA regions. Our analysis provides evidence that the air-sea C<sub>ANT</sub> flux contribution to the C<sub>ANT</sub>  
216 storage and to the total air-sea CO<sub>2</sub> flux in the NA is lower than expected from ocean inversions.  
217 Advection is the main contribution to the C<sub>ANT</sub> storage rate north of 25°N. Practically, the entire air-sea  
218 C<sub>ANT</sub> uptake in the NA occurs in the subtropical region, where the contemporary air-sea CO<sub>2</sub> flux is  
219 mainly anthropogenic, whereas the natural component predominates in the subpolar region. The high-  
220 to-low NAO transition was followed by a decrease in the heat and C<sub>ANT</sub> transports into the subpolar  
221 region due to the weakening of the MOC and the simultaneous decrease in the C<sub>ANT</sub> storage rate.

222 Because the anthropogenic contribution is a minor component of the contemporary air-sea CO<sub>2</sub> uptake  
223 in the subpolar region, we attribute the weakening of the contemporary air-sea CO<sub>2</sub> uptake to the  
224 decrease in natural CO<sub>2</sub> uptake. Our estimate of the decrease in natural CO<sub>2</sub> uptake inferred from the  
225 heat budget is in agreement with independent surface observations.

226 Finally, our study suggests that the long-term prediction of a reduction in the intensity of the  
227 MOC would be a positive climate-carbon feedback leading to a decrease in the C<sub>ANT</sub> storage.  
228 Concomitant air-sea heat loss reduction may lead to a decrease in the abiotic component of the natural  
229 CO<sub>2</sub> uptake, which would be an even more important feedback.

230

## 231 **Methods**

232 **C<sub>ANT</sub> estimations.** [C<sub>ANT</sub>] was computed using the back-calculation  $\phi C_{T^{\circ}}$  method<sup>42,43</sup> with an overall  
233 uncertainty of  $\pm 5.2 \mu\text{mol kg}^{-1}$ . [C<sub>ANT</sub>] in the subtropical region was estimated using the gridded  
234 CARINA dataset<sup>44</sup> and applying the  $\phi C_{T^{\circ}}$ , TrOCA<sup>45</sup> and TTD<sup>46</sup> methods. C<sub>ANT</sub> storage rates obtained  
235 from each of these methods were in good agreement. The final C<sub>ANT</sub> storage rate and its uncertainty for  
236 the subtropical region were calculated as the mean and the standard deviation of C<sub>ANT</sub> storage rates  
237 obtained from each method. For the subpolar, Nordic and Arctic boxes, the storage rates were from refs  
238 28, 31 and 47, respectively. Additional details are provided in the Supplementary Information.

239 **Transport computations across A25.** Absolute geostrophic currents were estimated using an inverse  
240 model constrained by subsurface ADCP (Acoustic Doppler Current Profiler) measurements and an  
241 overall mass conservation constraint<sup>21,22,24</sup>. The absolute velocity field is consistent with independent  
242 altimetry measurements<sup>24</sup> and estimates of the western boundary current transport<sup>48</sup> at the time of the  
243 OVIDE cruises. They are representative of the month of the cruise<sup>23</sup> and the seasonal variability was  
244 removed as explained in the Supplementary Information. Heat and C<sub>ANT</sub> transports were calculated

245 from current velocities perpendicular to the sections and from the potential temperature and  $C_{ANT}$   
246 fields, respectively. The uncertainties of the MOC, heat and  $C_{ANT}$  transports were estimated to be  $\pm 2$   
247 Sv, 0.05 PW and  $0.014 \text{ PgC}\cdot\text{y}^{-1}$ , respectively (see online Supplementary Information for full calculation  
248 details).

249 The errors of the mean transports (volume, heat or  $C_{ANT}$ ) across the A25 section were calculated  
250 as the standard deviation of the transport values divided by the square root of the number of transport  
251 values included in the estimate. Since only one transport estimate was available for the high NAO  
252 conditions, the error equals the standard deviation of the transports between 1997 and 2006, after  
253 removing a linear trend.

254  **$C_{ANT}$  transport at  $25^\circ\text{N}$ .** We used the estimates of  $C_{ANT}$  transports across  $25^\circ\text{N}$  reported in refs 4 and 7  
255 that were respectively obtained from hydrographic cruises carried out in 1992 and 1998 and from  $C_{ANT}$   
256 estimates based on a classic back-calculation method and on the  $C^*$  method. We rescaled both  
257 estimates to year 2004 by removing the effect of the inter-annual variability of the MOC in  $C_{ANT}$   
258 transports along  $25^\circ\text{N}$ . In addition, we corrected the MOC estimates for their intra-annual variability.  
259 The resulting value obtained after the rescaling was  $0.25 \pm 0.05 \text{ PgC}\cdot\text{y}^{-1}$ . Details on these computations  
260 and the uncertainty estimates are given in the Supplementary Information.

261 **Relationship between air-sea fluxes of heat and natural  $\text{CO}_2$ .** The linear regression of natural  $C_T$   
262 transports versus heat transports reported in Supplementary Table 4 for the A25 line has a slope of -  
263  $0.56 \pm 0.10 \text{ PgC}\cdot\text{y}^{-1}$  per PW ( $p < 0.05$ ). Assuming that the variability of heat and natural  $C_T$  transports  
264 over the sills and of accumulative terms are negligible<sup>29,49</sup>, this slope can be interpreted as a  
265 relationship between the air-sea flux of natural  $\text{CO}_2$  and the air-sea heat loss in the subpolar box. In the  
266 Nordic seas, a similar relationship is found between air-sea flux of natural  $\text{CO}_2$  and air-sea heat loss.  
267 Using the mean value of the observed air-sea  $\text{CO}_2$  uptake ( $0.09 \pm 0.01$  and  $0.11 \pm 0.06 \text{ PgC}\cdot\text{y}^{-1}$  as

268 reported in refs 1 and 50, respectively) and the heat loss given in Fig. 3, we obtained a value of -  
269  $0.5 \pm 0.1 \text{ PgC} \cdot \text{yr}^{-1}$  of air-sea flux per PW of heat loss in the Nordic seas. This relationship can also be  
270 applied to the natural  $\text{CO}_2$  air-sea fluxes of the Nordic Seas, since here the  $C_{\text{ANT}}$  air-sea flux is  
271 negligible, as shown in Fig. 3.

272

## 273 References

- 274 1. Takahashi, T. *et al.* Climatological mean and decadal change in surface ocean  $\text{pCO}_2$ , and net sea-  
275 air  $\text{CO}_2$  flux over the global oceans. *Deep-Sea Res. II* **56**, 554–577 (2009).
- 276 2. Sabine, C. L. *et al.* The oceanic sink for anthropogenic  $\text{CO}_2$ . *Science* **305**, 367–371 (2004).
- 277 3. Gruber, N. *et al.* Oceanic sources, sinks, and transport of atmospheric  $\text{CO}_2$ . *Glob. Biogeochem.*  
278 *Cycles* **23**, (2009).
- 279 4. Rosón, G., Ríos, A. F., Pérez, F. F., Lavin, A. & Bryden, H. L. Carbon distribution, fluxes, and  
280 budgets in the subtropical North Atlantic Ocean ( $24.5^\circ\text{N}$ ). *J. Geophys. Res.* **108**, 3144 (2003).
- 281 5. Keeling, R. F. & Peng, T.-H. Transport of Heat,  $\text{CO}_2$  and  $\text{O}_2$  by the Atlantic's Thermohaline  
282 Circulation. *Phil. Trans. R. Soc. Lond. B* **348**, 133–142 (1995). (1995) 348, 133-142 .
- 283 6. Mikaloff-Fletcher, S. E. *et al.* Inverse estimates of the oceanic sources and sinks of natural  $\text{CO}_2$   
284 and the implied oceanic carbon transport. *Glob. Biogeochem. Cycles* **21**, GB1010, 19 PP. (2007).
- 285 7. Macdonald, A. M., Baringer, M. O., Wanninkhof, R., Lee, K. & Wallace, D. W. R. A 1998–1992  
286 comparison of inorganic carbon and its transport across  $24.5^\circ\text{N}$  in the Atlantic. *Deep-Sea Res. II*  
287 **50**, 3041–3064 (2003).
- 288 8. Álvarez, M., Ríos, A. F., Pérez, F. F., Bryden, H. L. & Rosón, G. Transports and budgets of total  
289 inorganic carbon in the subpolar and temperate North Atlantic. *Glob. Biogeochem. Cycles* **17**, 1002  
290 (2003).

- 291 9. Quay, P. *et al.* Anthropogenic CO<sub>2</sub> accumulation rates in the North Atlantic Ocean from changes in  
292 the <sup>13</sup>C/<sup>12</sup>C of dissolved inorganic carbon. *Glob. Biogeochem. Cycles* **21**, GB1009 (2007).
- 293 10. Metzl, N. *et al.* Recent acceleration of the sea surface fCO<sub>2</sub> growth rate in the North Atlantic  
294 subpolar gyre (1993–2008) revealed by winter observations. *Glob. Biogeochem. Cycles* **24**,  
295 GB4004 (2010).
- 296 11. Watson, A. J. *et al.* Tracking the Variable North Atlantic Sink for Atmospheric CO<sub>2</sub>. *Science* **326**,  
297 1391–1393 (2009).
- 298 12. *The Hurrell NAO winter index is computed as the difference of surface atmospheric pressure*  
299 *between Iceland and Azores (timeseries values available at*  
300 *www.cgd.ucar.edu/cas/jhurrell/indices.html. In the early 90s (1989–1995) the 5-year mean ±*  
301 *standard deviation of this index was 3.3±0.8 indicating a high phase of the NAO. A low NAO phase*  
302 *period followed during the years 2002–2006, when the index value dropped to -0.1±0.6. Year 1996*  
303 *is characterized by negative NAO, and 1997 to 2000 by moderate positive NAO. This pattern is*  
304 *also observed when NAO index from SLP is computed in winter months.*
- 305 13. Patra, P. K. *et al.* Interannual and decadal changes in the sea-air CO<sub>2</sub> flux from atmospheric CO<sub>2</sub>  
306 inverse modeling. *Glob. Biogeochem. Cycles* **19**, GB4013 (2005).
- 307 14. Thomas, H. *et al.* Changes in the North Atlantic Oscillation influence CO<sub>2</sub> uptake in the North  
308 Atlantic over the past 2 decades. *Glob. Biogeochem. Cycles* **22**, GB4027 (2008).
- 309 15. Gruber, N., Keeling, C. D. & Bates, N. R. Interannual Variability in the North Atlantic Ocean  
310 Carbon Sink. *Science* **298**, 2374–2378 (2002).
- 311 16. Bates, N. R. Interannual variability of the oceanic CO<sub>2</sub> sink in the subtropical gyre of the North  
312 Atlantic Ocean over the last 2 decades. *J. Geophys. Res.* **112**, C09013, 26 PP. (2007).

- 313 17. Ullman, D. J., McKinley, G. A., Bennington, V. & Dutkiewicz, S. Trends in the North Atlantic  
314 carbon sink: 1992-2006. *Glob. Biogeochem. Cycles* **23**, (2009).
- 315 18. Kanzow, T. *et al.* Seasonal Variability of the Atlantic Meridional Overturning Circulation at  
316 26.5°N. *J. Clim.* **23**, 5678–5698 (2010).
- 317 19. Bryden, H. L., Longworth, H. R. & Cunningham, S. A. Slowing of the Atlantic meridional  
318 overturning circulation at 25° N. *Nature* **438**, 655–657 (2005).
- 319 20. Yashayaev, I. & Dickson, B. Transformation and Fate of Overflows in the Northern North Atlantic.  
320 *Arctic–Subarctic Ocean Fluxes* 505–526 (2008).
- 321 21. Lherminier, P. *et al.* Transports across the 2002 Greenland-Portugal Ovide section and comparison  
322 with 1997. *J. Geophys. Res.* **112**, C07003 (2007).
- 323 22. Lherminier, P. *et al.* The Atlantic Meridional Overturning Circulation and the subpolar gyre  
324 observed at the A25-OVIDE section in June 2002 and 2004. *Deep-Sea Res. I* **57**, 1374–1391  
325 (2010).
- 326 23. Treguier, A. M. *et al.* The North Atlantic Subpolar Gyre in Four High-Resolution Models. *J. Phys.*  
327 *Oceanogr.* **35**, 757–774 (2005).
- 328 24. Gourcuff, C., Lherminier, P., Mercier, H. & Le Traon, P. Y. Altimetry combined with hydrography  
329 for ocean transport estimation. *J. Atmos. Oceanic. Technol.* **29**, 1324-1336 (2011).
- 330 25. Böning, C. W., Scheinert, M., Dengg, J., Biastoch, A. & Funk, A. Decadal variability of subpolar  
331 gyre transport and its reverberation in the North Atlantic overturning. *Geophys. Res. Lett.* **33**,  
332 L21S01 (2006).
- 333 26. Mikaloff-Fletcher, S. E. M. *et al.* Inverse estimates of anthropogenic CO<sub>2</sub> uptake, transport, and  
334 storage by the ocean. *Glob. Biogeochem. Cycles* **20**, GB2002 (2006).

- 335 27. Tjiputra, J. F., Assmann, K. & Heinze, C. Anthropogenic carbon dynamics in the changing ocean.  
336 *Ocean Sci.* doi:10.5194/os-6-605-2010 (2010).
- 337 28. Pérez, F. F. *et al.* Trends of anthropogenic CO<sub>2</sub> storage in North Atlantic water masses.  
338 *Biogeosciences*, doi:10.5194/bg-7-1789-2010. (2010).
- 339 29. Hansen, B. & Østerhus, S. North Atlantic–Nordic Seas exchanges. *Prog. Oceanogr.* **45**, 109–208  
340 (2000).
- 341 30. Tanhua, T., Olsson, K. A. & Jeansson, E. Tracer Evidence of the Origin and Variability of Denmark  
342 Strait Overflow Water. *Arctic–Subarctic Ocean Fluxes* 475–503 (2008).
- 343 31. Jutterström, S. *et al.* Evaluation of anthropogenic carbon in the Nordic Seas using observed  
344 relationships of N, P and C versus CFCs. *Prog. Oceanogr.* **78**, 78–84 (2008).
- 345 32. Anderson, L. G., Olsson, K. & Chierici, M. A carbon budget for the Arctic Ocean. *Glob.*  
346 *Biogeochem. Cycles* **12**, 455–465 (1998).
- 347 33. Olsen, A. *et al.* Magnitude and Origin of the Anthropogenic CO<sub>2</sub> Increase and the <sup>13</sup>C Suess Effect  
348 in the Nordic Seas since 1981. *Glob. Biogeochem. Cycles* **20**, GB3027 (2006).
- 349 34. Körtzinger, A., Quay, P. D. & Sonnerup, R. E. Relationship between anthropogenic CO<sub>2</sub> and the  
350 <sup>13</sup>C Suess effect in the North Atlantic Ocean. *Glob. Biogeochem. Cycles* **17**, 1005 (2003).
- 351 35. Kieke, D. *et al.* Changes in the pool of Labrador Sea Water in the subpolar North Atlantic.  
352 *Geophys. Res. Lett.* **34**, L06605 (2007).
- 353 36. Våge, K., Pickart, R. S., Moore, G. W. K. & Ribergaard, M. H. Winter Mixed Layer Development  
354 in the Central Irminger Sea: The Effect of Strong, Intermittent Wind Events. *J. Phys. Oceanogr.* **38**,  
355 541–565 (2008).

- 356 37. Steinfeldt, R., Rhein, M., Bullister, J. L. & Tanhua, T. Inventory changes in anthropogenic carbon  
357 from 1997–2003 in the Atlantic Ocean between 20°S and 65°N. *Glob. Biogeochem. Cycles* **23**,  
358 GB3010 (2009).
- 359 38. Corbière, A., Metzl, N., Reverdin, G., Brunet, C. & Takahashi, T. Interannual and decadal  
360 variability of the oceanic carbon sink in the North Atlantic subpolar gyre. *Tellus B* **59**, 168–178  
361 (2007).
- 362 39. Schuster, U. & Watson, A. J. A variable and decreasing sink for atmospheric CO<sub>2</sub> in the North  
363 Atlantic. *J. Geophys. Res.* **112**, C11006 (2007).
- 364 40. Visbeck, M. *et al.* The ocean's response to North Atlantic Oscillation variability. *Geophysical*  
365 *Monograph Series* **134**, 113–145 (2003).
- 366 41. Schmitz, W. J. & Richardson P. L. On the sources of the Florida Current. *Deep-Sea Research* **38**,  
367 **Suppl. 1**, S389–S409 (1991).
- 368 42. Pérez, F. F. *et al.* Temporal variability of the anthropogenic CO<sub>2</sub> storage in the Irminger Sea.  
369 *Biogeosciences*, doi:10.5194/bg-5-1669-2008 (2008).
- 370 43. Vázquez-Rodríguez, M. *et al.* Anthropogenic carbon distributions in the Atlantic Ocean: data-  
371 based estimates from the Arctic to the Antarctic. *Biogeosciences* doi:10.5194/bg-6-439-2009  
372 (2009).
- 373 44. Velo, A. *et al.* A multiparametric method of interpolation using WOA05 applied to anthropogenic  
374 CO<sub>2</sub> in the Atlantic. *Sci. Mar.* **74**, 21–32 (2010).
- 375 45. Touratier, F., Azouzi, L. & Goyet, C. CFC-11,  $\Delta^{14}\text{C}$  and  $^3\text{H}$  tracers as a means to assess  
376 anthropogenic CO<sub>2</sub> concentrations in the ocean. *Tellus B* **59**, 318–325 (2007).
- 377 46. Waugh, D. W., Hall, T. M., McNeil, B. I., Key, R. & Matear, R. J. Anthropogenic CO<sub>2</sub> in the  
378 oceans estimated using transit time distributions. *Tellus B* **58**, 376–389 (2006).

- 379 47. Tanhua, T. *et al.* Ventilation of the Arctic Ocean: Mean ages and inventories of anthropogenic CO<sub>2</sub>  
380 and CFC-11. *J. Phys. Oceanogr.* **114**, C01002 (2009).
- 381 48. Daniault, N., Lherminier, P. & Mercier, H. Circulation and Transport at the Southeast Tip of  
382 Greenland. *J. Phys. Oceanogr.* **41**, 437–457 (2011).
- 383 49. Jeansson, E. *et al.* The Nordic Seas carbon budget: Sources, sinks, and uncertainties. *Glob.*  
384 *Biogeochem. Cycles* **25**, GB4010,16 PP. (2011).
- 385 50. Skjelvan, I. *et al.* A review of the inorganic carbon cycle of the Nordic Seas and Barents Sea. *The*  
386 *Nordic Seas: An Integrated Perspective Oceanography, Climatology, Biogeochemistry, and*  
387 *Modeling* **158**, 157–175 (2005).
- 388

389 Correspondence to: F. F. Pérez ([fiz.perez@iim.csic.es](mailto:fiz.perez@iim.csic.es)).

### 390 **Acknowledgements**

391 This work was supported by the Spanish Ministry of Sciences and Innovation and co-founded  
392 by the Fondo Europeo de Desarrollo Regional 2007-2012 (FEDER) through the CATARINA project  
393 (CTM2010-17141) and through EU FP7 project CARBOCHANGE “Changes in carbon uptake and  
394 emissions by oceans in a changing climate” which received funding from the European  
395 Commission’s 7<sup>th</sup> Framework Programme EU under grant agreement no. 264879. The OVIDE  
396 research project was co-funded by the IFREMER, CNRS/INSU and LEFE. H.M. was supported by  
397 CNRS and PL by IFREMER. M.V-R. was funded by CSIC I3P Predoctoral Grant program (I3P-  
398 BPD2005).

### 399 **Author Contributions**

400 All authors contributed extensively to the work presented in this paper. F.F.P., H.M. and A.F.R.  
401 designed the research. F.F.P., H.M., M.V-R, A.V., P.L. and A.F.R. analysed the physical and chemical  
402 data. H.M. and P.L. estimated the currents and thermohaline fields. F.F.P., M.V-R, A.V. and G.R.  
403 determined the anthropogenic CO<sub>2</sub> concentrations and storage rates. H.M., F.F.P., P.L. and A.F.R.  
404 estimated the uncertainties. F.F.P., H.M., M.V-R., P.C.P. and A.F.R wrote the paper. All authors  
405 discussed the results and implications and commented on the manuscript at all stages.

### 406 **Author Information**

407 The authors declare no competing financial interests. Supplementary Information is linked to  
408 the online version of the paper at [www.nature.com/nature](http://www.nature.com/nature). Reprints and permissions information is  
409 available online at <http://www.nature.com/nature/reprints>. Correspondence and request for materials  
410 should be addressed to F.F.P.

411

412 **Figure Legends**

413

414 **Figure 1 | Circulation and  $C_{ANT}$  in the North Atlantic.** **a)**  $C_{ANT}$  storage rates ( $\text{mol}\cdot\text{C}\cdot\text{m}^{-2}\cdot\text{y}^{-1}$ ) and the  
415 main currents and water masses participating in the MOC (black line: North Atlantic Current (NAC),  
416 Gulf Stream (GS); grey line: Labrador Sea Water –LSW-, white lines: Denmark Strait and Iceland-  
417 Scotland Overflow Waters –DSOW and ISOW). The 25°N, FOUREX and OVIDE section tracks are  
418 indicated (blue dotted lines); **b)** Vertical distribution of  $[C_{ANT}]$  ( $\mu\text{mol}\cdot\text{kg}^{-1}$ ) during the OVIDE 2004  
419 cruise. Potential temperature ( $^{\circ}\text{C}$ ; white lines) and the isopycnal  $\sigma_1 = 32.10$  (solid black line) separating  
420 the upper and lower limbs of MOC are also shown.

421

422 **Figure 2 | Integrated transports of volume, heat and  $C_{ANT}$  across the A25 section (Greenland -**  
423 **Portugal) in 0.01 density bins.** **a)** Volume transport ( $10^6 \text{ m}^3 \text{ s}^{-1}$ ); **b)** Heat transport (PW); **c)**  $C_{ANT}$   
424 transport ( $\text{kmol} \text{ s}^{-1}$ ). Color lines refer to years 1997 (grey), 2002 (yellow), 2004 (red) and 2006 (blue).  
425 The  $\sigma_1 = 32.10$  horizon (solid black horizontal lines) represents the boundary between the upper and  
426 lower limbs of the MOC. NAC = North Atlantic Current, uLSW = upper Labrador Sea Water, cLSW =  
427 classical Labrador Sea Water.

428

429 **Figure 3 |  $C_{ANT}$  budget in the North Atlantic referred to 2004.** The upper box represents the NA and  
430 the lower boxes represent the four sub-regions. The horizontal arrows show the lateral transports of  
431  $C_{ANT}$  in  $\text{PgC}\cdot\text{y}^{-1}$  (blue font) and heat transports in PW (maroon font). The black numbers in the boxes  
432 are the  $C_{ANT}$  storage rates in  $\text{PgC}\cdot\text{y}^{-1}$ . The vertical arrows show the anthropogenic (numbers in blue  
433 font) and contemporary (red font) air-sea  $\text{CO}_2$  fluxes in  $\text{PgC}\cdot\text{y}^{-1}$ . Errors appear in grey font. The surface  
434 area ( $\text{m}^2$ ) of each region and the latitudinal boundaries between them are shown.

435

436 **Figure 4 | Variability of the  $C_{ANT}$  budget in the subpolar box during high NAO (1997) and low**  
437 **NAO (2002-2006).** Arrow and number formats are the same as in Figure 3, except for the numbers in  
438 green font that are the natural air-sea  $CO_2$  fluxes in  $PgC \cdot y^{-1}$ , and in maroon font that are the air-sea heat  
439 flux in PW. Areal  $C_{ANT}$  storage rates ( $mol-C \cdot m^{-2} \cdot y^{-1}$ ) are also given. For 1997, the heat budget includes  
440 a heat accumulation rate of  $0.10 \pm 0.05$  PW.

441

442

## Supplementary Information

### Atlantic Ocean CO<sub>2</sub> uptake reduced by weakening of the meridional overturning circulation

Fiz F. Pérez<sup>1</sup>, Herlé Mercier<sup>2</sup>, Marcos Vázquez-Rodríguez<sup>1</sup>, Pascale Lherminier<sup>3</sup>, Anton Velo<sup>1</sup>, Paula C. Pardo<sup>1</sup>, Gabriel Rosón<sup>4</sup> and Aida F. Ríos<sup>1</sup>

<sup>1</sup> Instituto de Investigaciones Marinas, IIM-CSIC, Vigo, Spain. <sup>2</sup> CNRS, Laboratoire de Physique des Océans, UMR6523, CNRS, Ifremer, IRD, UBO, Plouzané, France. <sup>3</sup> Ifremer, Laboratoire de Physique des Océans, UMR6523, CNRS, Ifremer, IRD, UBO, Plouzané, France. <sup>4</sup> Faculty of Marine Sciences, University of Vigo, Campus Lagoas-Marcosende, 36200 Vigo, Spain.

#### 1. Anthropogenic CO<sub>2</sub> computation and inventory estimate

We used three methods for computing anthropogenic CO<sub>2</sub> ( $C_{ANT}$ ) from in situ measurements: the TTD (Transit Time Distribution<sup>1</sup>), TrOCA<sup>2</sup> and  $\phi C_T^\circ$  (refs 3,4) methods. On the basis of the variables needed to compute  $C_{ANT}$ , these methods can be classified into two groups: The carbon-based methods (TrOCA and  $\phi C_T^\circ$ ), which typically require measurements of  $C_T$ ,  $A_T$ , oxygen, temperature, salinity and eventually nutrients, and the TTD method that uses CFC-11 or CFC-12 measurements as proxies of the anthropogenic CO<sub>2</sub> signal. A summary presentation of those methods of  $C_{ANT}$  computation has been given in ref. 3. We applied the TrOCA and  $\phi C_T^\circ$  methods to the GLODAP and CARINA databases. The  $C_{ANT}$  estimates obtained by applying the TTD method to the GLODAP dataset<sup>1</sup> were downloaded from the following website: [https://jshare.johnshopkins.edu/dwaugh1/public\\_html/Cant/](https://jshare.johnshopkins.edu/dwaugh1/public_html/Cant/). The uncertainties in  $C_{ANT}$  are  $\pm 6.2$ ,  $\pm 5.2$ , and  $\pm 5.0 \mu\text{mol kg}^{-1}$  for the TrOCA,  $\phi C_T^\circ$  and TTD methods, respectively<sup>3</sup>. They depend on the specific assumptions of each methodology and on the corresponding analytical errors of the variables involved.

To compute the  $C_{ANT}$  inventories in the subtropical box, we first adapted the fields of  $[C_{ANT}]$  obtained from the CARINA/ GLODAP database to the WOA09 grid using a multi-parametric interpolation algorithm<sup>5</sup>. Second, we computed the specific (per unit area) inventories (Fig 1a) by vertically integrating the  $[C_{ANT}]$  on the WOA09 grid and, finally, we did a spatial (surface)

integration to determine the inventories. The uncertainties in these inventories were calculated by randomly propagating over depth<sup>3</sup> a  $5 \mu\text{mol kg}^{-1}$  standard error of the  $C_{\text{ANT}}$  estimate. The inventory uncertainties were equal to  $\pm 1 \text{ mol-C m}^{-2}$  and  $\pm 2 \text{ mol-C m}^{-2}$  when the vertical integration went down to 3000 m and 6000 m depths, respectively. For the subtropical box (surface area =  $16.6 \cdot 10^{12} \text{ m}^2$ ), the estimated inventories are  $17.3 \pm 0.3$ ,  $18.7 \pm 0.3$  and  $16.8 \pm 0.4 \text{ PgC}$  for the TrOCA,  $\phi C_T^\circ$  and TTD methods respectively, that yield an average value of  $17.6 \pm 0.6 \text{ PgC}$ . In the subpolar box we relied on the  $C_{\text{ANT}}$  inventories computed in Perez et al. (2010; ref. 6).

## 2. $C_{\text{ANT}}$ storage rate in the subtropical box

Based on previous works<sup>7-9</sup> we considered a transient steady state of the  $C_{\text{ANT}}$  distribution in the subtropical NA. Accordingly, the storage rate of  $C_{\text{ANT}}$  was computed from the inventory multiplied by the annual rate of increase  $k_t$  ( $C_{\text{ANT}}$  storage rate =  $k_t * C_{\text{ANT}}$  inventory). The value of  $k_t$  ( $0.016 \pm 0.001 \text{ y}^{-1}$ ) was calculated as the rate of increase of  $[C_{\text{ANT}}]$  in the mixed layer divided by  $[C_{\text{ANT}}]$  in the mixed layer considering that the evolution of  $[C_{\text{ANT}}]$  in the winter mixed layer follows the exponential increase of atmospheric  $\text{CO}_2$  (refs 8, 9). The storage rates in the subtropical box were estimated in  $0.299 \pm 0.0045$ ,  $0.277 \pm 0.005$  and  $0.269 \pm 0.006 \text{ PgC} \cdot \text{y}^{-1}$  by the TrOCA,  $\phi C_T^\circ$ , and TTD methods, respectively. The value in the budget presented in Fig.3 was obtained as the mean value and standard error ( $0.280 \pm 0.011 \text{ PgC} \cdot \text{y}^{-1}$ ) of the ensemble of storage rates from all three  $C_{\text{ANT}}$  methods together. Also,  $k_t$  was used as a rescaling factor of  $C_{\text{ANT}}$  storage rates and  $C_{\text{ANT}}$  transports to years 2004 and 1997, whenever these were reported for other years.

## 3. $C_{\text{ANT}}$ Storage rate in the subpolar box

Because the subpolar box includes areas of water mass formation<sup>10,11</sup>, the assumption of a steady transient tracer distribution is not valid<sup>9,12</sup> there. This is mostly due to the fact that the thickness of the main water mass (LSW) in this region has a strong variability associated with the

NAO<sup>10,11</sup>. This variability drives strong changes in the  $C_{ANT}$  storage rates<sup>6,8,12</sup> due to the formation of LSW during the period of low NAO compared to the exceptional convection activity during the period of high NAO<sup>8</sup>. For the budget presented in Fig. 4, we relied on ref. 6 who indicated a drop in the storage rate in the “OVIDE Box” from  $0.054 \pm 0.006 \text{ PgC} \cdot \text{y}^{-1}$  during the high NAO period (1991-1997) to  $0.026 \pm 0.004 \text{ PgC} \cdot \text{y}^{-1}$  during the low NAO period (1998-2006). These results are in agreement with those inferred from CFC data<sup>8</sup>. On average, the  $C_{ANT}$  storage rate for the subpolar box referred to 2004 is  $0.045 \pm 0.004 \text{ PgC} \cdot \text{y}^{-1}$  (Fig 3). The budget for the high NAO period in Fig. 4a was calculated by re-computing the storage rate in ref. 6 using the area of a subpolar box south-bounded by the FOUREX track. The storage rate was estimated at  $0.083 \pm 0.008 \text{ PgC} \cdot \text{y}^{-1}$ .

#### **4. $C_{ANT}$ transports through the sills**

The isopycnal  $\sigma_0 = 27.80$  separates the northward flowing NA water masses entering the Nordic Seas [Eastern North Atlantic Central Water (ENACW), Modified North Atlantic Central Water (MNACW), Greenland-Iceland Inflow Water (GIIW)] in the upper layers from the southward flowing water masses [Denmark Strait Overflow Water (DSOW), Iceland Scotland Overflow Water (ISOW) and East Greenland Current (EGC)] in the lower layer (Supplementary Table 1). The volume transports and associated errors were taken from the literature<sup>15</sup>.

#### **5. $C_{ANT}$ storage in the Nordic Seas**

Given the average  $C_{ANT}$  inventory of 1.2 PgC estimated from chlorofluorocarbon data<sup>13</sup>, a storage rate of  $C_{ANT}$  of  $0.018 \pm 0.004 \text{ PgC} \cdot \text{y}^{-1}$  was obtained using a  $k_t$  of  $0.016 \pm 0.001 \text{ y}^{-1}$  (refs 8, 9). This storage rate value is in agreement with a recent estimation<sup>14</sup>.

**Supplementary Table 1** -  $C_{ANT}$  transports through the sills.

Water Mass	Volume Transport (Sv)	$[C_{ANT}]$ ( $\mu\text{mol kg}^{-1}$ )	$C_{ANT}$ Transport referred to 2004 ( $\text{kmol s}^{-1}$ )
DSOW	-3 $\pm$ 1	30 $\pm$ 3	-89
ISOW	-3 $\pm$ 1	28 $\pm$ 3	-84
EGC	-1.8 $\pm$ 0.2	37 $\pm$ 3	-66
ENACW	3.85 $\pm$ 1	49 $\pm$ 4	189
MNACW	3.85 $\pm$ 1	51 $\pm$ 4	196
GIIW	0.8 $\pm$ 0.2	40 $\pm$ 3	32
<b>Total</b>	0.7 $\pm$ 2.0		166 $\pm$ 51 $\text{kmol s}^{-1}$ 0.063 $\pm$ 0.019 $\text{PgC}\cdot\text{y}^{-1}$

*EGC (East Greenland Current), ENACW (Eastern North Atlantic Central Water), MNACW (Modified North Atlantic Central Water) and GIIW (Greenland-Iceland Intermediate Water)*

The  $[C_{ANT}]$  in the upper layer were estimated assuming that surface waters are saturated with  $\text{CO}_2$  (ref. 16). The  $[C_{ANT}]$  for the DSOW was taken from the literature<sup>13</sup> and  $[C_{ANT}]$  for the ISOW was estimated from water mass decomposition (Supplementary Table 2; refs 17, 18). The  $[C_{ANT}]$  data for the rest of the water masses flowing over the sills were taken from previous studies<sup>13</sup>. Additionally, since our study is referenced to years 1997 (high NAO) or 2004 (low NAO),  $C_{ANT}$  transports over the sills were rescaled by applying the previously derived  $k_t$  factor of  $0.016 \pm 0.001 \text{ y}^{-1}$ , and we obtained transports of  $0.057 \pm 0.018 \text{ PgC}\cdot\text{y}^{-1}$  and  $0.063 \pm 0.019 \text{ PgC}\cdot\text{y}^{-1}$  for 1997 and 2004, respectively. These results fully corroborate recent transport estimates ( $0.062 \pm 0.014 \text{ PgC}\cdot\text{y}^{-1}$  for 2002; ref. 14).

**Supplementary Table 2.-** Water masses properties and  $[C_{ANT}]$  over the Nordic sills.

Water Mass	Mixing %	$\theta$ range ( $^{\circ}\text{C}$ )	$\theta$ avg. ( $^{\circ}\text{C}$ )	Salinity	$[C_{ANT}]$ referred to 2004 ( $\mu\text{mol kg}^{-1}$ )
NSAIW+NSDW	50	<0.4	0	34.885	10.9
MEIW	25	<3	2	34.80	40.4
MNAW	25	8	7.75	35.15	49.2
ISOW	100		2.44	34.93	28.0

*NSAIW (Norwegian Sea Arctic Intermediate Water), NSDW (Norwegian Sea Deep Water), MEIW (Modified East Icelandic Water) MNAW (Modified North Atlantic Water)*

## 6. Arctic Seas $C_{ANT}$ storage and transports

Based on earlier estimates<sup>19</sup>, we considered an average value of  $2.9 \pm 0.4$  PgC for the  $C_{ANT}$  inventory in the Arctic Seas referred to 2005. By applying the same  $k_t$  factor of  $0.016 \pm 0.001$   $y^{-1}$ , we estimated a  $C_{ANT}$  storage rate of  $0.043$  PgC $\cdot y^{-1}$  referenced to 2004. The  $C_{ANT}$  transport between the Arctic and Nordic Seas in 1991 was estimated to be  $0.031 \pm 0.004$  PgC $\cdot y^{-1}$  northward<sup>20</sup>. Rescaling this value to 2004, a  $C_{ANT}$  transport of  $0.039 \pm 0.008$  PgC $\cdot y^{-1}$  was obtained. This result agrees with recent transport estimates of  $0.040 \pm 0.019$  PgC $\cdot y^{-1}$  referenced to 2002 (ref. 14). The  $C_{ANT}$  transport through Davis Strait was neglected. The net  $C_{ANT}$  transport from the Pacific to the Atlantic Ocean through the Bering Strait was obtained from previous works<sup>21,22</sup>.

## 7. Transports and uncertainties at 25°N

The seasonal variability of the MOC at 25°N has been recently evaluated<sup>23</sup> on the basis of the RAPID measurements. It has shown that the seasonal variability of the MOC is forced by the wind stress curl variability at the eastern boundary and affects the upper mid-ocean transport ( $T_{UMO}$ ) in a narrow band close to the eastern boundary. The  $[C_{ANT}]$  in this region ( $[C_{ANT}]_{TUMO}$ , Supplementary Table 3) was obtained from previous works<sup>24,25</sup> and the seasonal correction of  $T_{CANT}$  was modeled as  $\Delta T_{UMO} \cdot [C_{ANT}]_{TUMO}$ , where  $\Delta T_{UMO}$  is seasonal transport anomaly.  $\Delta T_{UMO}$  was estimated<sup>23</sup> at  $0.9 \pm 0.9$  and  $-2 \pm 0.9$  Sv for the 1992 and 1998 cruises, respectively. The rescaled  $C_{ANT}$  transports were hence computed applying the following equation:

$$T_{CANT}(2004) = (T_{CANT}(1992/1998) - \Delta T_{UMO} \cdot [C_{ANT}]_{TUMO}) \cdot (1 + k_t)^{\Delta y} \cdot MOC_{RAPID} / MOC_{CORR}$$

where  $MOC_{COR}$  and  $MOC_{RAPID}$  are the de-seasonalized and long-term averaged MOC ( $18.7 \pm 2.1$  Sv) as given by ref. 23.  $\Delta y$  is the time lapse (in years) between 2004 and 1992 or 1998. The final uncertainties were computed as the standard deviation of an ensemble generated by random perturbations of the 1992/1998  $C_{ANT}$  transports,  $\Delta T_{UMO}$ ,  $[C_{ANT}]_{\Delta T_{UMO}}$  and  $k_t$ . The value of  $0.25 \pm 0.05$   $PgC \cdot y^{-1}$  for  $C_{ANT}$  transport at  $25^\circ N$  is obtained as the mean between the 1992 and 1998 estimates, rescaled to 2004 and de-aliased from the seasonal variability. The most important contributions to the uncertainties are the initial uncertainties<sup>24,25</sup>, while the rescaling of the MOC is practically negligible.

**Supplementary Table 3.-** Deseasonalized  $C_{ANT}$  transport. ( $1 \text{ PgC} \cdot \text{yr}^{-1} = 2642 \text{ kmol/s}$ )

Year	$C_{ANT}$ transport (kmol/s)	2004 $C_{ANT}$ transport (kmol/s)	$\Delta T_{UMO}$ (Sv)	$C_{ANT} T_{UMO}$ ( $\mu\text{mol} \cdot \text{kg}^{-1}$ )	$MOC_{COR}$ (Sv)	$(1 + k_t)^{\Delta y}$	Long term 2004 $C_{ANT}$ transport ( $PgC \cdot y^{-1}$ )
1992	$630 \pm 200$	$725 \pm 200$	$0.9 \pm 0.9$	$45 \pm 3$	18.5	$1.213 \pm 0.015$	$0.28 \pm 0.08$
1998	$449 \pm 159$	$610 \pm 160$	$-2 \pm 0.9$	$51 \pm 3$	18.1	$1.066 \pm 0.005$	$0.23 \pm 0.06$

## 8. Transports and uncertainties at A25

The MOC, heat,  $C_{ANT}$  and natural  $C_T$  transports across the A25 section are given in Supplementary Table 4. The natural  $C_T$  was computed as the difference between measured (total)  $C_T$  and  $C_{ANT}$ . The natural  $C_T$  transports were used to establish a relationship between air sea fluxes of heat and natural  $CO_2$  for the subpolar box (see Methods). The associated uncertainties in Supplementary Table 4 are the standard deviations of an ensemble of 100 tracer transport estimates obtained by random perturbations of the volume transports and tracer fields scaled using the error covariance matrix of the velocity field given by the inverse model<sup>15</sup> and the uncertainties in natural  $C_T$  and  $C_{ANT}$  concentrations ( $6 \mu\text{mol} \cdot \text{kg}^{-1}$  each). The natural  $C_T$  and  $C_{ANT}$  transport uncertainties were equal to  $0.026$  and  $0.014 \text{ PgC} \cdot \text{yr}^{-1}$ , respectively. These uncertainties are very similar to those that would be obtained using the approximate method proposed by ref. 26.

The seasonal variability of the MOC along A25 was evaluated using the high-resolution DRAKKAR ocean general circulation model<sup>27</sup>. During the OVIDE cruises the seasonal anomaly was not significant ( $0.0\pm 0.5$ ) because these cruises were conducted in June, when the seasonal anomaly is at its minimum. On the contrary, the FOUREX occupation in September 1997 did need a seasonal correction of  $+2.0\pm 0.5$  Sv. The vertical gradient of the transport of  $[C_{ANT}]$  is not affected by the seasonal cycle<sup>28</sup> and we assumed that the seasonal variability of the vertical gradient of the transport of heat and natural  $C_T$  is also negligible. So, we corrected for the seasonal variability of MOC transports from refs 29 and 30 by linearly rescaling the transports by the ratio  $\langle MOC \rangle / MOC$  obtained in the model, where  $\langle MOC \rangle$  is the annual value and MOC the monthly value (Supplementary Table 4).

**Supplementary Table 4.-**  $C_{ANT}$  and natural  $C_T$  transports through A25 section

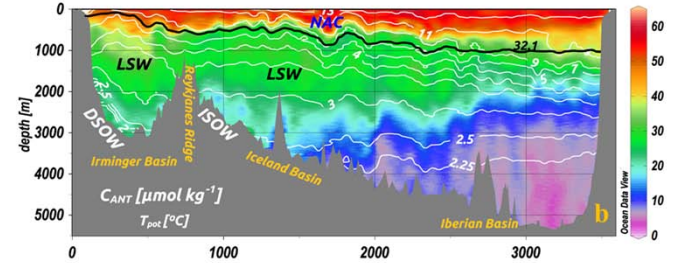
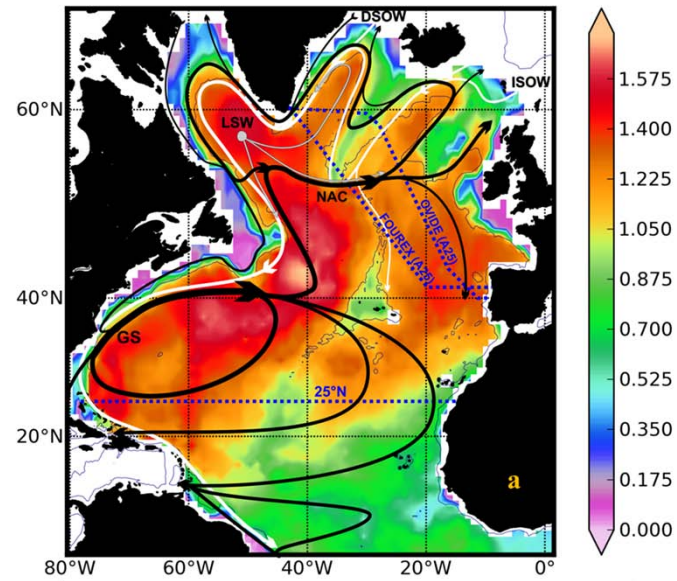
<b>Cruise</b>	<b>MOC (Sv)</b>	<b>Heat (PW)</b>	<b><math>C_{ANT}</math> (PgC·yr<sup>-1</sup>)</b>	<b>Natural <math>C_T</math> (PgC·yr<sup>-1</sup>)</b>
<b>4X 1997</b>	20.5	$0.76\pm 0.09$	$0.110\pm 0.014$	$-0.352\pm 0.026$
<b>Ov 2002</b>	16.2	$0.44\pm 0.05$	$0.077\pm 0.014$	$-0.207\pm 0.026$
<b>Ov 2004</b>	16.4	$0.50\pm 0.05$	$0.087\pm 0.014$	$-0.265\pm 0.026$
<b>Ov 2006</b>	11.2	$0.29\pm 0.05$	$0.058\pm 0.014$	$-0.079\pm 0.026$

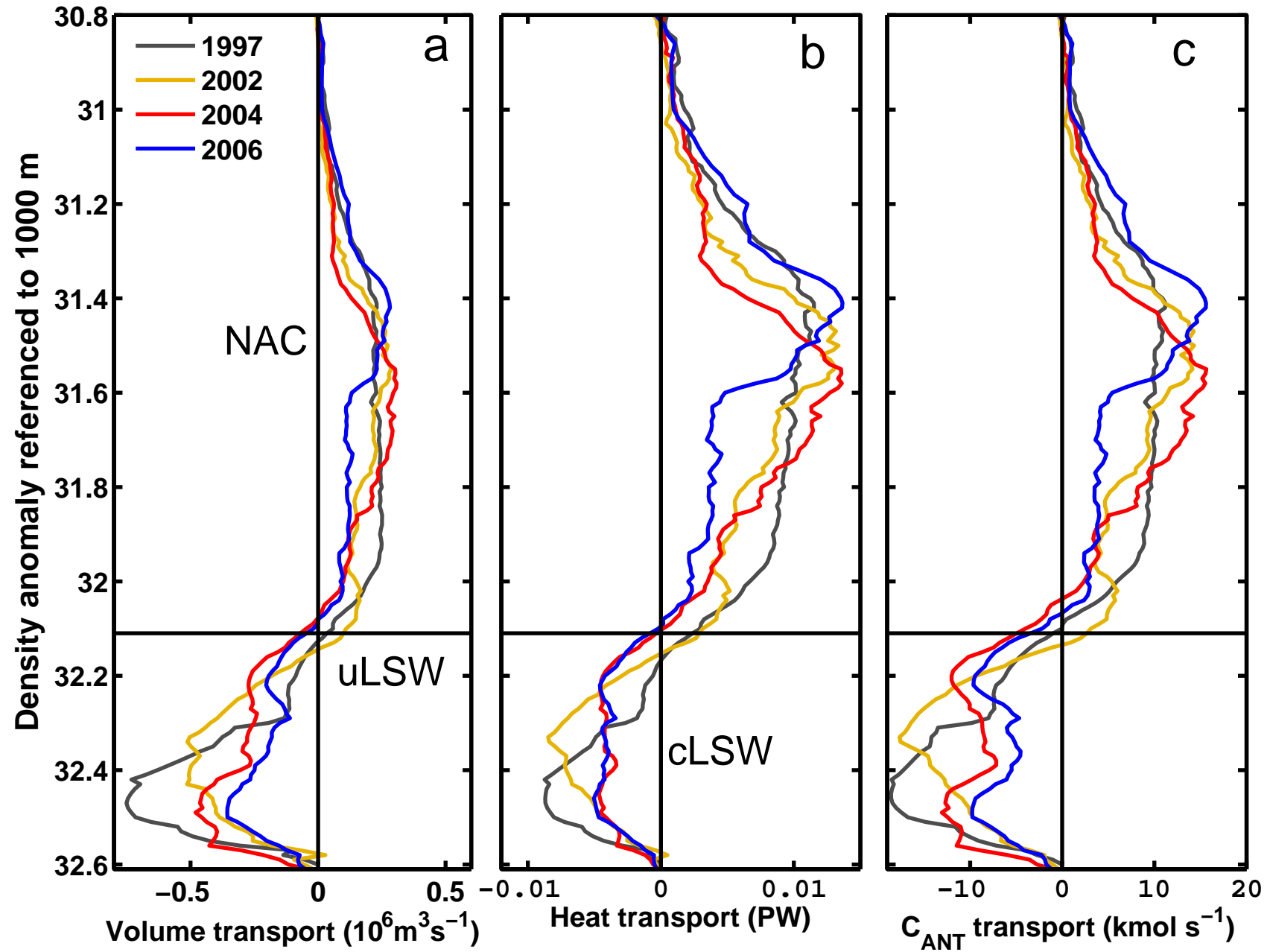
## 9. Supplementary references

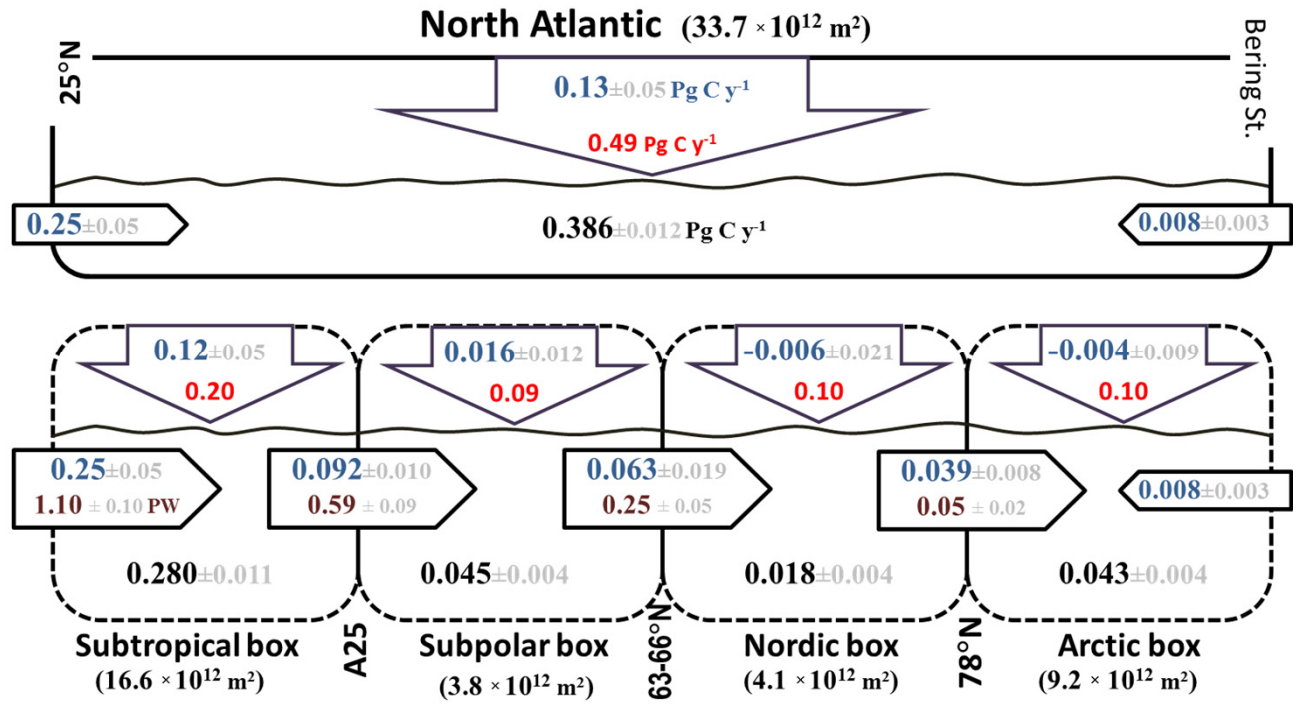
1. Waugh, D. W., Hall, T. M., McNeil, B. I., Key, R. & Matear, R. J. Anthropogenic CO<sub>2</sub> in the oceans estimated using transit time distributions. *Tellus B* **58**, 376–389 (2006).
2. Touratier, F., Azouzi, L. & Goyet, C. CFC-11,  $\Delta^{14}\text{C}$  and  $^3\text{H}$  tracers as a means to assess anthropogenic CO<sub>2</sub> concentrations in the ocean. *Tellus B* **59**, 318–325 (2007).
3. Vázquez-Rodríguez, M. *et al.* Anthropogenic carbon distributions in the Atlantic Ocean: data-based estimates from the Arctic to the Antarctic. *Biogeosciences* doi:10.5194/bg-6-439-2009 (2009).
4. Vázquez-Rodríguez, M., Padin, X. A., Ríos, A. F., Bellerby, R. G. J. & Pérez, F. F. An upgraded carbon-based method to estimate the anthropogenic fraction of dissolved CO<sub>2</sub> in the Atlantic Ocean. *Biogeosciences Discussions* doi:10.5194/bgd-6-4527-2009 (2009).
5. Velo, A. *et al.* A multiparametric method of interpolation using WOA05 applied to anthropogenic CO<sub>2</sub> in the Atlantic. *Sci. Mar.* **74**, 21–32 (2010).
6. Pérez, F. F. *et al.* Trends of anthropogenic CO<sub>2</sub> storage in North Atlantic water masses. *Biogeosciences* doi:10.5194/bg-7-1789-2010 (2010).
7. Keeling, C. D. & Bolin, B. The simultaneous use of chemical tracers in oceanic studies I. General theory of reservoir models. *Tellus* **19**, 566–581 (2010).
8. Steinfeldt, R., Rhein, M., Bullister, J. L. & Tanhua, T. Inventory changes in anthropogenic carbon from 1997–2003 in the Atlantic Ocean between 20°S and 65°N. *Glob. Biogeochem. Cycles* **23**, GB3010 (2009).
9. Tanhua, T. *et al.* Changes of anthropogenic CO<sub>2</sub> and CFCs in the North Atlantic between 1981 and 2004. *Glob. Biogeochem. Cycles* **20**, GB4017, 13 PP. (2006).
10. Yashayaev, I. & Dickson, B. Transformation and Fate of Overflows in the Northern North Atlantic. *Arctic–Subarctic Ocean Fluxes* 505–526 (2008).
11. Kieke, D. *et al.* Changes in the pool of Labrador Sea Water in the subpolar North Atlantic. *Geophys. Res. Lett.* **34**, L06605 (2007).
12. Pérez, F. F. *et al.* Temporal variability of the anthropogenic CO<sub>2</sub> storage in the Irminger Sea. *Biogeosciences* doi:10.5194/bg-5-1669-2008 (2008).
13. Jutterström, S. *et al.* Evaluation of anthropogenic carbon in the Nordic Seas using observed relationships of N, P and C versus CFCs. *Progress In Oceanography* **78**, 78–84 (2008).
14. Jeansson, E. *et al.* The Nordic Seas carbon budget: Sources, sinks, and uncertainties. *Glob. Biogeochem. Cycles* **25**, GB4010, 16 PP. (2011).
15. Lherminier, P. *et al.* The Atlantic Meridional Overturning Circulation and the subpolar gyre observed at the A25-OVIDE section in June 2002 and 2004. *Deep-Sea Res. I* **57**, 1374–1391 (2010).
16. Tanhua, T., Olsson, K. A. & Jeansson, E. Tracer Evidence of the Origin and Variability of Denmark Strait Overflow Water. *Arctic–Subarctic Ocean Fluxes* 475–503 (2008).
17. Fogelqvist, E. *et al.* Greenland–Scotland overflow studied by hydro-chemical multivariate analysis. *Deep-Sea Res. I* **50**, 73–102 (2003).

18. Hansen, B. *et al.* The Inflow of Atlantic Water, Heat, and Salt to the Nordic Seas Across the Greenland–Scotland Ridge. *Arctic–Subarctic Ocean Fluxes* 15–43 (2008).
19. Tanhua, T. *et al.* Ventilation of the Arctic Ocean: Mean ages and inventories of anthropogenic CO<sub>2</sub> and CFC-11. *J. Geophys. Res.* **114**, C01002 (2009).
20. Anderson, L. G., Olsson, K. & Chierici, M. A carbon budget for the Arctic Ocean. *Glob. Biogeochemical Cycles* **12**, 455–465 (1998).
21. Macdonald, A. M., Baringer, M. O., Wanninkhof, R., Lee, K. & Wallace, D. W. R. A 1998–1992 comparison of inorganic carbon and its transport across 24.5°N in the Atlantic. *Deep-Sea Res. II* **50**, 3041–3064 (2003).
22. Mikaloff Fletcher, S. E. *et al.* Inverse estimates of anthropogenic CO<sub>2</sub> uptake, transport, and storage by the ocean. *Glob. Biogeochem. Cycles* **20**, GB2002 (2006).
23. Kanzow, T. *et al.* Seasonal Variability of the Atlantic Meridional Overturning Circulation at 26.5°N. *J. Clim.* **23**, 5678–5698 (2010).
24. Rosón, G., Rios, A. F., Pérez, F. F., Lavin, A. & Bryden, H. L. Carbon distribution, fluxes, and budgets in the subtropical North Atlantic Ocean (24.5°N). *J. Geophys. Res.* **108**, 3144 (2003).
25. Macdonald, A. M., Baringer, M. O., Wanninkhof, R., Lee, K. & Wallace, D. W. R. A 1998–1992 comparison of inorganic carbon and its transport across 24.5°N in the Atlantic. *Deep-Sea Res. II* **50**, 3041–3064 (2003).
26. Ganachaud, A., Wunsch, C., Marotzke, J. & Toole, J. Meridional overturning and large-scale circulation of the Indian Ocean. *J. Geophys. Res.* **105**, 26117–26,134 (2000).
27. Barnier, B. *et al.* Impact of partial steps and momentum advection schemes in a global ocean circulation model at eddy-permitting resolution. *Ocean Dyn.* **56**, 543–567 (2006).
28. Biastoch, A., Völker, C. & Böning, C. W. Uptake and spreading of anthropogenic trace gases in an eddy-permitting model of the Atlantic Ocean. *J. Geophys. Res.* **112**, C09017 (2007).
29. Lherminier, P. *et al.* Transports across the 2002 Greenland-Portugal Ovide section and comparison with 1997. *J. Geophys. Res.* **112**, C07003 (2007).
30. Gourcuff, C., Lherminier, P., Mercier, H. & Le Traon, P. Y. Altimetry combined with hydrography for ocean transport estimation. *J. Atmos. Oceanic. Technol.* **29** 1324–1336 (2011).

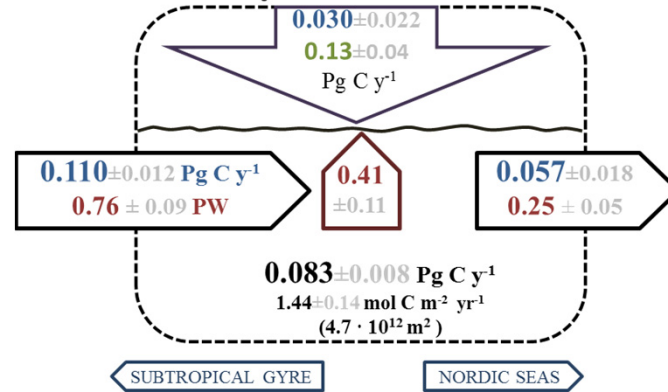
$C_{ANT}$  Storage rates ( $\text{mol-C}\cdot\text{m}^{-2}\cdot\text{y}^{-1}$ )







### Subpolar box 1997



### Subpolar box 2004

